SCANDAL – A facility for elastic neutron scattering studies in the 50–130 MeV range

J. Klug[a], J. Blomgren[a1], A. Ataç[a], B. Bergenwall[a], S. Dangtip[a], K. Elmgren[a], C. Johansson[a], N. Olsson[a], A.V. Prokofiev[a,j], J. Rahm[a], O. Jonsson[b], L. Nilsson[b], P.-U. Renberg[b], P. Nadel-Turonski[c], A. Ringbom[d], A. Oberstedt[e], F. Tovesson[e], C. Le Brun[f], J.F. Lecolley[f], F.R. Lecolley[f], M. Louvel[f], N. Marie[f], C. Schweitzer[f], C. Varignon[f], Ph. Eudes[g], F. Haddad[g], M. Kerveno[g], T. Kirchner[g], C. Lebrun[g], L. Stuttgé[h], I. Slypen[i], A.N. Smirnov[j], R. Michel[k], S. Neumann[k], U. Herpers[l]

[a] *Department of Neutron Research, Uppsala University, Sweden*
[b] *The Svedberg Laboratory, Uppsala University, Sweden*
[c] *Department of Radiation Sciences, Uppsala University, Sweden*
[d] *Swedish Defence Research Establishment (FOA), Stockholm, Sweden*
[e] *Department of Technology and Science, Örebro University, Sweden*
[f] *LPC, ISMRA et Université de Caen, CNRS/IN2P3, France*
[g] *SUBATECH, Université de Nantes, CNRS/IN2P3, France*
[h] *IReS, Strasbourg, France*
[i] *Institute de Physique Nucleaire, Université Catholique de Louvain, Belgium*
[j] *V.G. Khlopin Radium Institute, St. Petersburg, Russia*
[k] *Zentrum für Strahlenschutz und Radioökologie, Universität Hannover, Germany*
[l] *Abteilung Nuklearchemie, Universität zu Köln, Germany*

Abstract

A facility for detection of scattered neutrons in the energy interval 50–130 MeV, SCANDAL (SCAttered Nucleon Detection AssembLy), has recently been installed at the 20–180 MeV neutron beam facility of the The Svedberg Laboratory, Uppsala. It is primarily intended for studies of elastic neutron scattering, but can be used for the (n,p) and (n,d) reaction experiments as well. The performance of the spectrometer is illustrated in measurements of the (n,p) and (n,n) reactions on ^{1}H and ^{12}C. In addition, the neutron beam facility is described in some detail.

[1]Corresponding author. Tel. +46 18 471 3788. *E-mail address:* jan.blomgren@tsl.uu.se (J. Blomgren)

PACS: 28.20.Cz; 29.25.Dz; 29.30.-h; 29.30.Hs; 29.40.Cs; 29.40.Mc

Keywords: Neutron beam; neutron detection; active converter; CsI(Na) hodoscope; neutron scattering

---

1 Introduction

The interest in high-energy neutrons is rapidly growing. This is due to a number of potential large-scale applications involving fast neutrons, either having been identified or being under development. These applications primarily fall into three sectors; nuclear energy and waste, medicine and electronics effects.

The recent development of high-intensity proton accelerators has resulted in ideas to use subcritical reactors, fed by external spallation-produced neutrons, for transmutation of waste from nuclear power reactors or nuclear weapons material. This might result in less problematic waste material and/or energy production [1].

Conventional radiation treatment of tumours, i. e. by photons or electrons, is a cornerstone in modern cancer therapy. Some rather common types of tumours, however, cannot be treated successfully. For some of these, very good treatment results have been reached with neutron therapy, which is the largest non-conventional therapy world-wide [2, 3].

The last few years, it has become evident that electronics in aeroplanes suffer effects from cosmic-ray neutrons [4, 5]. The now most well-known effect is that a neutron can induce a nuclear reaction in the silicon substrate of a memory device, releasing a free charge, which in turn flips the memory content. This random reprogramming is obviously not wanted. Similar effects causing hardware damage have recently been identified also on ground level.

Neutrons at aircraft altitudes give a significant radiation dose to airplane personnel. This poses a relatively new dosimetry problem, which is currently under intensive investigation [6].

Finally, fundamental nuclear physics with intermediate-energy neutrons has recently got widespread attention due to the experimental studies of the absolute strength of the strong interaction in the nuclear sector, derived from neutron-proton scattering data [7].

Elastic neutron scattering plays a key role for the understanding of all these areas. The most important reason is that it allows a determination of the optical potential, which plays a decisive role in every microscopic calculation including neutrons in either the entrance or exit channel. In addition, the elastic cross section is also the largest of the individual partial cross sections contributing to the total cross section. In fact, a consequence of the optical model is that the elastic cross section must constitute at least half the total cross section.

All the applications mentioned above involve neutrons at much higher energies than for the traditional applied areas, e. g. nuclear power. Extensive evaluated data libraries have been established for the development of nuclear fission and fusion for energy production, which have a 20 MeV upper limit. Very little high-quality neutron-induced data exist above this energy. Only the total cross section [8] and the (n,p) reaction have been investigated extensively [9, 10]. There are high-quality neutron total cross section data on a series of nuclei all over this energy range. In addition, there are (n,p) data in the forward angular range at modest excitation energies available at a few energies and for a rather large number of nuclei.

Besides this, there are data on neutron elastic scattering from UC Davis at 65 MeV on a few nuclei [11]. Programmes to measure neutron elastic scattering have been proposed or begun at Los Alamos [12] and IUCF [13], with the former resulting in a thesis on data in the 5–30° range on a few nuclei [12]. The design of SCANDAL has been based on the experiences from the latter two projects.

Besides the role of elastic neutron scattering data for determining the neutron optical potential, there are also cases where they can be of direct use. Examples are in neutronics of spallation systems, including accelerator-driven transmutation cores, and fast-neutron cancer therapy, where 10–15 % of the dose comes from elastic neutron scattering.

All these research areas are represented at the neutron beam facility of the The Svedberg Laboratory (TSL). The facility has previously been described in a NIM publication [14]. Major recent upgrades in the neutron production motivate a renewed description of it, which is found in section 2. An overview of the experimental area is given in section 3, and the SCANDAL setup is described in section 4. Section 5 is devoted to experimental tests of the performance of the device, while the experimental programme is discussed in section 6, and finally, a summary and the conclusions are presented in section 7.

2 Neutron beam production

2.1 Neutron production techniques above 50 MeV

Neutron beam facilities above 50 MeV have traditionally been of two types; white sources and quasi-monoenergetic. White spallation sources have been used at Los Alamos [15] and Paul Scherrer Institute [16], and a new source is presently being installed at CERN [17]. Typically, the energy-integrated flux is significantly larger than for monoenergetic sources, on the expense that the flux per energy unit is much smaller. For elastic neutron scattering measurements, i. e. the scope of this paper, this smaller flux per energy unit is a clear disadvantage. This is illustrated by the fact that no data on elastic neutron scattering at intermediate energies have been published from white sources.

Monoenergetic sources are, like the Uppsala facility, in most cases employing the ^{7}Li(p,n) reaction. Such installations have been operated at UC Davis [18], IUCF [19], TRIUMF [20], NAC [21], TIARA [22], UCL [23], and RIKEN [24].

Recently, a novel technique has been developed at IUCF to produce tagged neutrons at a cooler ring [25]. This technique can be used to provide neutron beams with well-defined energy and intensity, but with the drawback that the intensity is very poor. A programme is underway to measure neutron-proton scattering, for which the intensity is sufficient, while it is inadequate for elastic scattering from nuclei.

Finally, the D(p,n) reaction has been extensively used to produce intense neutron beams with a slightly worse intrinsic resolution than the ^{7}Li(p,n) reaction, but with the advantage that reasonably polarized neutrons can be obtained. The limited beam resolution, however, prevents resolved studies of (polarized) elastic neutron scattering from nuclei.

2.2 The TSL neutron beam

An overview of the neutron beam facility at the The Svedberg Laboratory (TSL) is presented in fig. 1. Protons from the cyclotron impinge on a neutron production target from the left. After the target, the remaining proton beam is bent into a beam dump tunnel. A narrow neutron beam is defined by a system of three collimators. The major experimental devices are installed in a separate hall. The different parts are given detailed descriptions below.

Lithium targets of 100–800 mg/cm^2 thickness (2-15 mm), enriched to 99.98 % in ^{7}Li, are mounted in a remotely controlled water-cooled stainless-steel rig with four target holders, each with a diameter of 26 mm. One of the target positions contains a fluorescent screen viewed by a TV camera, which is used for beam alignment and focussing. Targets can be changed without breaking the vacuum; a vacuum lock reduces the exposure of the lithium targets to air to a few seconds. Previously, a cold trap was located close to the lithium target arrangement. Increased pumping capacity has made this cold trap unnecessary.

After passage of the target, the proton beam is deflected in two magnets and bent into an 8 m long tunnel, where it is focussed onto a water-cooled graphite beam dump. The integrated current from this Faraday cup is used for proton beam monitoring, which is also a relative monitoring of the neutron beam. An efficient dumping of the high-intensity proton beam is important for various reasons. A high beam transmission through the magnet elements reduces the irradiation around the beam tubes, making activation a smaller problem. In addition, the reliability of the proton current for relative neutron intensity monitoring improves.

A low-cost system has been installed to handle automatically the high-intensity beams in the beam dump line. It is based on placing electrically insulated 1 mm

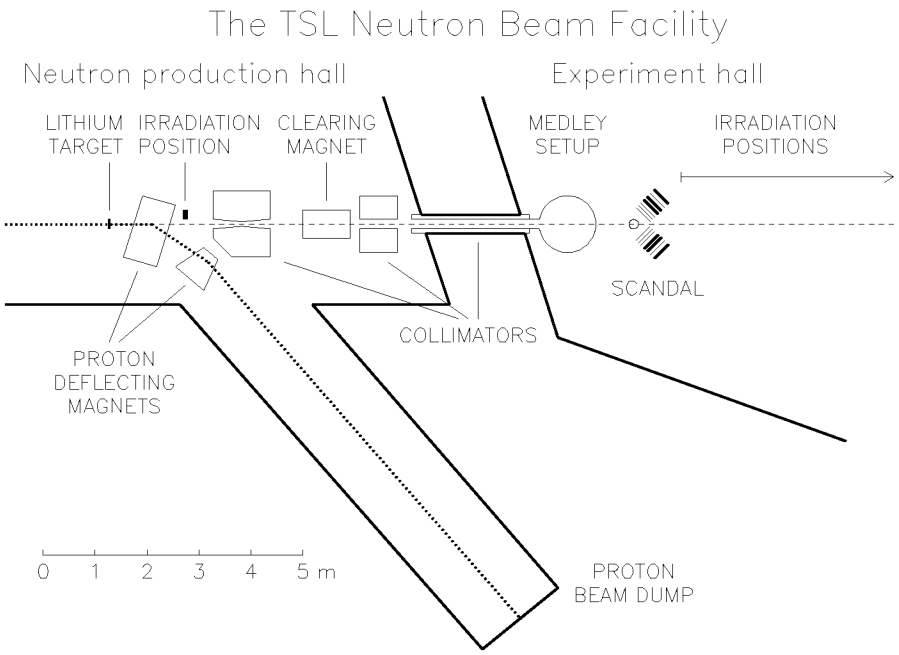

Figure 1: Overview of the Uppsala neutron beam facility.

stainless-steel pins vertically along the diameter of the beam tube in the path of the beam at two positions in the bending section. The beam profile is measured by scanning the beam with an upstream steering magnet. The beam is centered on the two pins by an automatic routine. An example of measured profiles for 180 MeV protons with and without production target is shown in fig. 2, which was obtained by scanning the preceding bending magnet current from 135 to 150 A. The effect of inserting the target is clearly visible. The centroid has shifted due to the lower energy in the beam after having passed it, and the width has increased due to energy and angular straggling.

The neutron beam produced in the forward direction is geometrically defined by a system of three collimators. The first one consists of a 1.1 m long iron cylinder of revolver type with four axial holes of different diameter. The cylinder is remotely controlled to collimate the neutron beam to solid angles of 60, 80, or 100 μsr. The fourth hole has the beam tube diameter, and can be used e. g. for alignment purposes when free sight through the collimator is required. The collimators are doubly conical in shape, with a central waist defining the solid angle.

The second collimator is 0.8 m thick and consists of iron and paraffin slabs, while the third one, about 2 m thick, is made of iron only. Neither of these two collimators shape the neutron beam, but serve as scrapers of the beam halo from

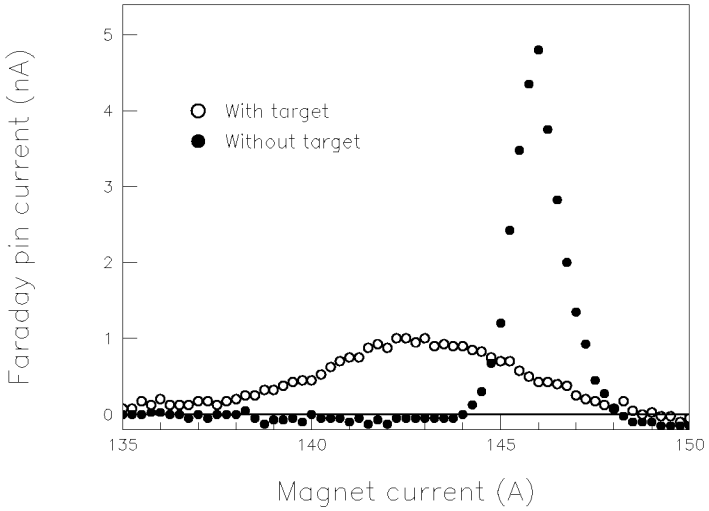

Figure 2: Example of a measured beam profile. The open and filled circles shows the profile with and without a lithium target, respectively.

the first collimator. The third collimator is conical in shape, with entrance and exit diameters of 60 and 75 mm, respectively. It is located in a wall separating the neutron-production area and the main experimental hall, and it also contains a beam shutter.

Protons passing through the lithium target have a small probability to pick up an electron and become hydrogen atoms, which are not deflected by the magnet after the target. For some experiments, this H^0 flux can be a problem. If so, a 1 mm thick aluminium valve after the first collimator can be closed, which results in H^0 breakup, and a dipole after the valve is used to clean the beam.

All the neutron production and collimation takes place in vacuum. The first major installation in the experimental hall, MEDLEY, is part of the vacuum system, which is terminated by a 0.1 mm stainless-steel foil at the exit of the MEDLEY scattering chamber.

In applications where the proton contamination of the beam has to be minimal, the aluminium valve and the clearing magnet described above can be used, with the valve terminating the vacuum, i.e. the MEDLEY exit foil is removed and the neutrons pass through the downstream fraction of the neutron beam line in air. With such precautions, the charged particle contamination of the neutron beam has been measured to be about 10^{-5}.

A prominent feature of the neutron production facility is the very good shield-

ing between the dumping and the experimental area, which gives low experimental background. The long distance between the neutron production and experiment area allows rejection of low-energy neutrons by time-of-flight techniques. A fast switching magnet upstream the neutron production facility allows it to be run in beam-share mode with other experiments at the laboratory, making very efficient use of the beam possible.

2.3 High-intensity irradiation facility

The main experimental devices are installed in a separate hall, well shielded from the neutron production. There is, however, one notable exception. Activation experiments can benefit from higher intensities and require very little space. A neutron irradiation facility for activation targets of maximum diameter 25 mm and length 60 mm is available 1.9 m downstream the neutron production target, located just after the proton bending magnet. It makes use of neutrons produced at an angle about 1° off the initial beam axis, and it does not interfere with other ongoing experiments further downstream.

2.4 Beam intensity monitors

Relative monitoring is provided by the proton beam Faraday cup (see above). In addition, absolute monitoring of the neutron fluence is obtained from a fission detector, based on thin-film breakdown counters (TFBCs) [26]. It consists of a double-sided ^{nat}U target and two TFBCs placed close to the target surfaces at its both sides. The fissile layers are deposited onto a 0.1 mm thick aluminium foil. The diameters of the fissile layers and the sensitive surfaces of the TFBCs are about 36 mm. The detectors and the target are placed in a non-vacuum aluminium chamber for electrical shielding and mechanical protection of the detectors. The device includes also a pulse amplifier placed in a separate box.

Depending on the required counting rate and the statistical accuracy, it is possible to use either one of the detectors or both of them simultaneously. The single-side mode is useful for neutron energies in the 20–100 MeV range when the proton beam current is in the range of a few μA. The double-side mode provides maximum sensitivity of the monitor, which is useful in the 100–180 MeV range where proton beam currents are commonly in the range of a few hundred nA.

Because of the nature of TFBC operation [27], detectors of this type can sustain only a limited number of breakdowns. Thus, for reliable and long-time operation of a TFBC, its counting rate should not exceed what is required to get a reasonably small statistical error. Under normal conditions this means about one breakdown per second, or a few thousand counts per hour. The tentative lifetime of the TFBC under such conditions is about 1500 proton μA·hours. The counting rate can be

optimized by adjusting the monitor sensitivity, which can be regulated within a rather wide range by varying the applied voltages or by using different targets, as well as by selecting the optimum mode of operation, i.e. single- or double-sided. The absolute uncertainties in the measured neutron fluence are about 10 %.

2.5 Neutron beam characteristics

The ^{7}Li(p,n) reaction produces a neutron spectrum consisting of a full-energy peak and a continuum of neutrons at lower energies, roughly evenly distributed in energy. The intensity is approximately equally distributed on these two regions. The full-energy peak is due to excitation of the ground state and first excited state (E_X = 0.43 MeV) in ^{7}Be. The energy of it is slightly lower than the initial proton energy ($Q = -1.6$ MeV), and the width is primarily given by the thickness of the lithium target. Typically, widths in the 1–4 MeV region have been used.

The intensity of the full-energy peak over the full beam area with the 60 μsr solid angle collimator is $5 \cdot 10^4$ neutrons per mm ^{7}Li target and μA of incident proton beam. The cyclotron is operated in isochronous mode up to 100 MeV, with proton beam intensities up to about 5 μA. Above 100 MeV, it employs frequency modulation, which results in much less intensity, about 200 nA at the highest proton energy, 180 MeV. To some extent this loss in proton intensity is compensated for by a lower energy loss in lithium, allowing thicker targets to be used for the same energy resolution. Thereby a loss in proton beam intensity by a factor ten gives a neutron intensity reduction by a factor five.

Low-energy neutrons can be rejected by time-of-flight techniques, which is illustrated in fig. 3. The pulse width of the cyclotron is about 4 ns, which corresponds to a neutron energy interval of 13 MeV at 100 MeV neutrons 8 m from the production target. This is the main reason for the incomplete rejection.

For a 100 MeV energy and a 8 m flight path to the experimental setup, the first three wrap-around neutron energies are at 24, 11 and 6 MeV. Thereby, for all measurements of ejectiles with higher energies, this is normally not a problem. For some experiments, however, this can be a major obstacle. A system to increase the pulse separation with preserved intensity is under consideration. One possible technique might be to select pulses with a sweeping system at an early stage of the acceleration where the activation of the lost beam is small, combined with an increased ion source intensity.

The magnetic spectrometer LISA [14] has been used for characterization of the high-energy part of the neutron spectrum. By measuring the (n,p) reaction on CH_2 and pure carbon targets, the H(n,p) reaction spectrum can be constructed. Knowing the energy variation of the H(n,p) cross section, i.e. the *np* scattering cross section, the energy distribution of the incident neutrons can be derived. This technique has shown that the energy distribution within 40 MeV of the full-energy peak is

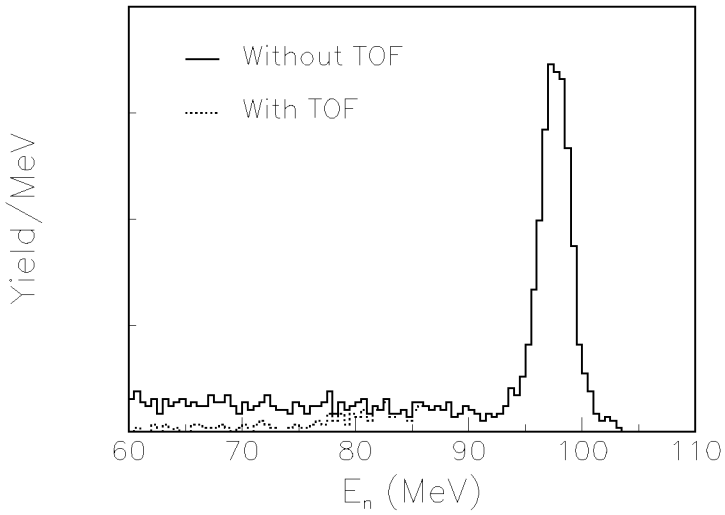

Figure 3: Reconstructed energy spectra of incoming neutrons, using a proton spectrum in the angular range $0 - 5°$ measured with the LISA magnetic spectrometer. The solid line shows the spectrum without time-of-flight conditions, and the dashed spectrum is obtained with such a cut.

in good agreement with the data on the ^{7}Li(p,n) reaction by Byrd and Sailor [28], while measurements at lower neutron energies have not been carried out with this method, due to the limited momentum bite of the magnetic spectrometer.

In fission measurements on fissile targets, like ^{235}U, wrap-around neutrons can be a major problem all the way down to zero energy. This has motivated an investigation of the low-energy neutron content in the beam. The measurements were based on time-of-flight (TOF) techniques in conjunction with neutron-induced fission reactions. Targets of ^{232}Th, ^{235}U, ^{238}U, and $^{\mathrm{nat}}$U were used in different runs. Fission fragments were detected by TFBCs with fast timing properties. The TFBCs were mounted close to the targets as sandwiches. In addition, one of the sandwiches with a ^{235}U target was surrounded by a 1 mm thick Cd foil. Since cadmium possesses a very high capture cross section at neutron energies below about 0.5 eV, the foil attenuated the neutron flux in this energy region by many orders of magnitude. On the other hand, neutrons with energies above about 10 eV interacted with the foil material with a probability of only 2–3 %. Thus, a comparison of data obtained with two ^{235}U targets with and without cadmium surrounding them allowed an estimation of the neutron flux in the near-thermal energy region.

As an example of the results, fig. 4 shows time spectra of fission events obtained

in the neutron production hall in the vicinity of the irradiation position described in section 2, with a peak neutron energy of 44 MeV. The spectra of ^{232}Th and ^{nat}U fission events reflect the high-energy part of the neutron spectrum, while the ones of ^{235}U are affected by wrap-around of low-energy neutrons. A comparison of the spectra obtained for ^{235}U targets with and without cadmium surrounding them, makes it evident that the neutron spectrum includes a measurable component at energies below 0.5 eV. Assuming a Maxwellian energy distribution for the low-energy component, its time-averaged flux was found to be about 1 % of the high-energy peak neutron flux. Similar investigations were made in the experimental hall. TOF spectra of fission events were obtained for ^{235}U and ^{238}U targets, placed alternately in the beam, and out of the beam. The resulting thermal/peak flux ratio was found to be not more than $2 \cdot 10^{-4}$.

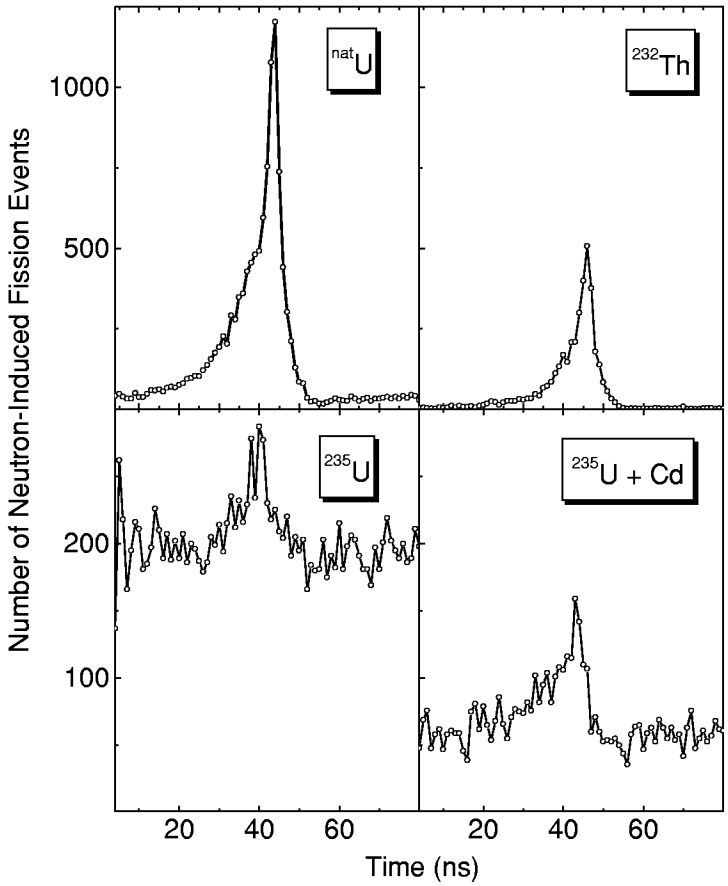

Figure 4: The fission reaction rate versus time measured in the neutron production hall. The peak neutron energy is 44 MeV (see the text for details).

The uniformity of the beam at the high-intensity irradiation position has been verified by activation techniques, where foils covering different regions of the beam spot were activated. No deviations from uniformity was found beyond a 4 % uncertainty given by statistics and the systematic uncertainty of the measurement.

3 Experimental area

The experimental hall contains three major devices. The Light Ion Spectrometer Assembly (LISA) is a magnetic spectrometer [14] for (n,p) studies. It has been used for extensive studies of the (n,p) reaction on nuclei in the $A = 9 - 208$ mass range [29, 30, 31, 32, 33, 34], and on precise experiments on np scattering [35, 36, 37, 38].

The MEDLEY detector array [39] has been designed for measurements of neutron-induced light-ion production cross sections of medical relevance, i. e. for fast-neutron cancer therapy and related dosimetry. It consists of eight particle telescopes, placed at 20–160 degrees with 20 degrees separation. Each telescope is a $\Delta E - \Delta E - E$ detector combination, with sufficient dynamic range to distinguish all charged particles from a few MeV up to about 130 MeV. All the equipment is housed in a 100 cm diameter scattering chamber, so that the charged particles can travel in vacuum.

The SCAttered Nucleon Detection AssembLy (SCANDAL) is primarily intended for studies of elastic neutron scattering, but can be used for the (n,p) and (n,d) reactions as well. It is described in some detail below.

Finally, there is about 8 m of neutron beam line between SCANDAL and the beam dump. This is used for other kinds of experiments, like fast-neutron fission [40], studies of neutron-induced electronics failures [41, 42] or dosimetry research.

4 The SCANDAL setup

4.1 General layout

The setup is primarily intended for studies of elastic neutron scattering, i. e., (n,n) reactions. The neutron detection is accomplished via conversion to protons by the H(n,p) reaction. In addition, (n,p) reactions in nuclei can be studied by direct detection of protons. This is also used for calibration of the setup. Therefore, it has been designed for a quick and simple change from one mode to the other.

The device is illustrated in fig. 5. It consists of two identical systems, in most cases located on each side of the neutron beam. The design allows the neutron beam to pass through the drift chambers on the left side of each setup, making low-background measurements close to zero degrees feasible.

In neutron detection mode, each arm consists of a 2 mm thick veto scintillator for fast charged-particle rejection, a neutron-to-proton converter which is a 10 mm thick plastic scintillator, a 2 mm thick plastic scintillator for triggering, two drift chambers for proton tracking, a 2 mm thick ΔE plastic scintillator which is also part of the trigger, and an array of CsI detectors for energy determination. The trigger is provided by a coincidence of the two trigger scintillators, vetoed by the front scintillator. If used for (n,p) studies, the veto and converter scintillators can be removed, and additional drift chambers can be mounted if desired.

In neutron detection mode, a large solid angle of protons emitted from the converter is of crucial importance to get reasonable statistics. This implies that the distance from the converter to the CsI hodoscope should be as short as possible, while proton tracking is required. Inserting a third drift chamber would improve the proton tracking, both in position accuracy and in overall efficiency, but at the expense that the proton solid angle decreases dramatically. Therefore, only two drift chambers are used, but the design allows a third chamber to be installed if desired.

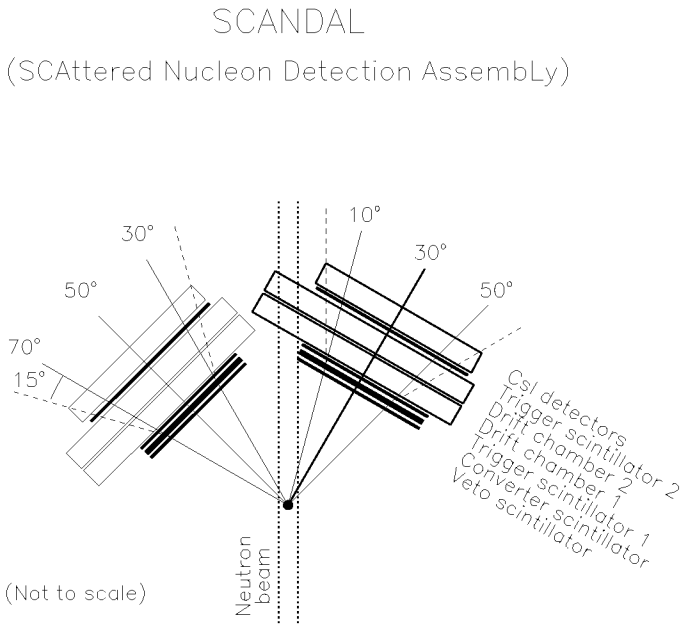

Figure 5: Schematic figure of the SCANDAL setup.

4.2 Converter scintillator

Neutrons have to be converted to charged particles to be detected. We have chosen the H(n,p) reaction for neutron-to-proton conversion because it has a large cross section (above 50 mb/sr at small angles in the 50–130 MeV range), and it populates no excited states in a residual nucleus. Two main approaches can in principle be used; passive or active converters.

Active converters have the advantage that they can be thicker, because the proton straggling on the way out of the scintillator can be measured and compensated for. The maximum thickness of an active converter is thereby set by the energy resolution of the detector. A typical plastic scintillator has a resolution in the 10–15 % range, and the proton energy loss is about 0.7–1.0 MeV/mm for 70–100 MeV protons. Thereby, a converter thickness of 10 mm gives up to 10 MeV deposited energy, and the resolution contribution is henceforth up to about 1 MeV.

The most frequently used converters contain hydrogen and carbon, which allows unambiguous measurements up to 12 MeV excitation energy. For higher excitation energies, the ^{12}C(n,p) channel opens in the converter, and therefore a unique identification of the target excitation is no longer possible. This is obviously not a problem for elastic scattering, or inelastic scattering to low-lying states, but complicates experiments where low-energy neutron emission is under study. This problem is, however, present both for active and passive converters.

The problems above can be circumvented by using a passive liquid hydrogen converter, but the technique is both non-trivial and expensive. Another prize to pay is that the converter must be an order of magnitude thinner for the same resolution. Based on these discussions, we have chosen to use active plastic scintillator converters.

4.3 CsI hodoscope

The setup has in total 24 CsI(Na) detectors, 12 in each system. These detectors are trapezoidal in shape, 30 cm high with a $7 \cdot 7$ cm^2 cross section area at the PM tube end, and a $5 \cdot 5$ cm^2 area in the other end. By placing them in alternating directions, a 72 cm wide CsI hodoscope has been installed. This geometric shape is not optimal; the crystals were manufactured for another experiment and have been recycled. The shape makes the light output position-dependent, and this effect has to be compensated for in the offline analysis.

An average energy resolution of 3.0 MeV has been demonstrated for 77 MeV protons. As each detector has an individual resolution, it may deviate significantly from this figure; ranging from less than 2 MeV up to around 5 MeV in the worst case.

CsI crystals are frequently doped with tallium, which allows particle identifica-

tion through pulse-shape analysis. Doping with sodium, like in the present case, makes the crystals much more resistent to radiation damage, at the expense that the particle identification capability is lost. In the present application, this is not an important matter. The only particle identification needed is proton-deuteron separation, which is easily accomplished with $\Delta E - E$ techniques.

4.4 Drift chambers

The drift chambers serve two main purposes; they improve the angular resolution and they allow rejection of spurious events. The H(n,p) cross section close to zero degrees is rather flat over several degrees in the lab system. This effect, combined with the rather large front-area of the CsI's, makes the effective subtended angular range for each detector quite large. This would be a major contribution to the energy and angular resolution without proton tracking.

Furthermore, the Q-value for ^{12}C(n,p) is -12.6 MeV. Thus, at forward angles energy detection can isolate the protons which are due to conversion via H(n,p). At about 20° conversion angle, the proton energies from the two processes are the same, and thereby it can no longer be determined whether the energy lost was due to excitations in the neutron scattering sample or in the conversion. By applying a maximum opening angle criterion on the conversion (see fig. 5), such problems can be avoided.

Sufficient angular information is obtained by placing drift chambers between the converter and the CsI's. Hence, the conversion point is well determined. This has also the potential of allowing rejection of spurious events. With this technique, the remaining contribution to the angular resolution is the width of the neutron beam (or the scattering sample). The only way to improve the angular resolution further would be to use a narrower beam or target, but that would be at the expense of count rate.

The drift chambers are of double sense-wire type with two-dimensional readout. The horizontal coordinate is determined from one out of 40 drift cells, and the vertical from one out of eight. Each drift cell is 24 mm wide, making the total active area $960 \cdot 192$ mm^2. The position within each cell is determined by measuring the electron drift time. The position resolution is 0.3 mm (FWHM) for each coordinate. The chambers are described in more detail in reference [43].

The maximum detection efficiency possible to obtain for a single coordinate is about 98 %, when defining a good event as having at least one hit in a plane. There is, however, a non-zero probability of cross-talk between adjacent wires. For most events, the time information can be used to select the correct wire, but not all. In elastic neutron scattering measurements with SCANDAL, these double-hit events have to be rejected. By lowering the high voltage biasing the chambers, the nominal efficiency is slightly reduced, but the fraction of double hits is reduced even more,

increasing the figure-of-merit for good events. For optimum conditions, the efficiency for a single coordinate is in the 90–97 % range.

4.5 Multitarget

For (n,p) measurements, a multitarget arrangement can be used to increase the target content without impairing the energy resolution. This multitarget box allows up to seven targets to be mounted simultaneously, interspaced with multi-wire proportional counters. In this way it is possible to determine in which target the reaction took place, and corrections for energy loss in the subsequent targets can be applied. In (n,n) measurements, the multitarget is placed empty upstreams the scattering target, and used as charged-particle veto. A more detailed description can be found in reference [14].

4.6 Resolution

The energy resolution in neutron mode has contributions from the neutron beam (1.2 MeV at FWHM), the converter (1.4 MeV), the two trigger scintillators (0.3 MeV each), straggling in non-detector materials (0.25 MeV), kinematics (1.2 MeV), and the CsI detectors (3.0 MeV). This makes a total excitation-energy resolution of 3.7 MeV in elastic scattering measurements. This resolution is comparable with the distance from the ground state to the first excited state in most of the nuclei of interest, e. g., ^{12}C (4.4 MeV), ^{16}O (6.1 MeV), ^{40}Ca (3.3 MeV), ^{90}Zr (1.8 MeV), and ^{208}Pb (2.6 MeV).

The angular resolution is solely due to the neutron beam and target width. With the present setup dimensions and a 5 cm wide sample, it is about 1.4° (rms). The angular resolution is most crucial at small angles, where the cross section falls very rapidly. For these angles, the cross section is also very large, and thereby a narrow strip target could be used to improve the angular resolution, without making the total beam time considerably longer.

4.7 Solid angle and count rate

The solid angle subtended by each system in the proton detection mode is about 240 msr for a point target. Applying the maximum opening angle criterion on the second scattering in the converter (see above), required for neutron detection, makes the effective solid angle smaller – about 130 msr per setup at full coverage of the 15° cone. The conversion efficiency is then about $5 \cdot 10^{-4}$.

In a typical experiment, the two arms will be located such as to cover 10–50°, and 30–70°, respectively. For a one-week run on ^{208}Pb, the total number of counts

for a one-degree angular bin is expected to be about 5 000 at 10°, and 1 at 70°, illustrating that the cross section falls off rapidly with angle.

4.8 Electronics and data acquisition

Each plastic scintillator has two PM tubes, mounted adjacent to each other on one of the longer, horizontal sides of the scintillator. The signals are lead to a remote counting room, where they are handled using mainly standard electronic units.

The signal from each plastic scintillator PM tube is split into an energy and a timing branch using a linear fan-in/fan-out. The pulse height of the energy signal is registered by a charge-integrating ADC (QDC), which is gated by a MASTER signal (see below).

The timing signal is fed to a constant fraction discriminator (CFD), which generates a stop signal for a TDC. In addition, for the veto and trigger PM tubes, a second CFD signal is utilized for event definition. A logic OR between the two PM tubes is used to define a hit in the respective detector. A logic AND between the two trigger (T1 and T2) signals, vetoed by the veto detector (V) signal, is used to define an event in the left- or right-side setup, i. e. a SCANDAL LEFT or SCANDAL RIGHT event. These signals are fed to a pattern unit to register which setup triggered the event. Furthermore, an OR between SCANDAL LEFT and SCANDAL RIGHT defines the MASTER signal, which announces the presence of an event in one of the setups. The MASTER signal causes a read-out of the system, starts the TDCs, and gates the energy signals (ADCs) and the pattern unit.

The CsI signals are processed by preamplifiers placed close to the detectors. After transport to the counting room, the signals are fed into a spectroscopic amplifier and registered by peak-sensing ADCs.

Drift chamber amplifiers and discriminators are mounted directly on the chambers. The output signals are fed to a LeCroy 4290 TDC system, situated in the experimental area, and read out by CAMAC.

The radiofrequency (RF) signal from the cyclotron is used as a time-of-flight reference signal, and is recorded as a stop signal in a TDC which is started by the MASTER signal. At the same time, the complementary of the RF signal is used to veto the OR unit that defines the MASTER signal; i. e., if there is no RF signal, no MASTER signal will be created. In addition to this, a computer busy signal from the data acquisition system (see below) acts as a veto on the MASTER signal.

A scaler unit is used to monitor the dead time of the data acquisition system and the intensity of the neutron beam. The number of pulses from a 100 Hz clock, both with and without a computer busy veto, is registered for the dead time determination, giving typical values of 5–10 %. Signals from the proton beam Faraday cup and the fission counter give two independent values of the neutron flux.

Data are recorded on an event-by-event basis using SVEDAQ, a general-purpose

data acquisition system employed at the TSL [44]. Data are read out through a CAMAC branch highway and sent to a VME-based event-builder. From the event-builder system, data are split into two independent branches; to an Exabyte tape station for recording, and to online analysis. A SUN workstation is used for online sorting, monitoring and control. Typical online spectra that can be displayed are pulse heights from scintillator detectors, time-of-flight (TOF) and drift chamber hit position distributions.

5 Experimental tests, data analysis and results

5.1 Experimental procedure

To investigate the characteristics of the SCANDAL setup and to illustrate the experimental procedures, we have performed measurements both in proton and in neutron detection mode, at a neutron beam energy of 96 MeV.

The proton mode runs were used for studies of the H(n,p), ^{12}C(n,p) and ^{12}C(n,d) reactions, as well as for calibration purposes. In order to get enough statistics for the calibration of all CsI detectors, each arm was consecutively placed at both sides of the beam, giving sufficient data for the six detectors closest to the beam at each setting.

In the (n,p) measurements, the multitarget box was filled with CH_2 targets of total thickness 0.26 mg/cm^2, and with carbon targets of total thickness 0.34 g/cm^2. A background run was made with the multitarget box containing only one CH_2 foil for reference.

In neutron mode, a carbon cylinder of 5 cm height and 5 cm diameter was used as a target, while the multitarget box was empty and acting as a charged-particle veto. Here, the angular ranges 10–50° and 30–70°, respectively, were covered by the two arms.

5.2 Proton mode test experiment

5.2.1 Energy calibration

For the analysis of both proton and neutron mode data, the scintillator detector pulse heights (PH) have to be converted into energy. This calibration is done using protons from H(n,p) reactions in one of the CH_2 foils in the multitarget box.

In the CsI cases, two calibration points are identified for each detector: a pedestal channel due to events detected in other CsIs, and thus associated with zero energy; and a H(n,p) proton peak. A centroid channel is found by fitting a Gaussian to the proton peak, and the deposited energy represented by that channel is obtained by calculating the energy loss of protons between the target and the CsI in question.

Assuming a linear correspondence between PH and energy gives a simple relation between these quantities. However, due to detector geometry and local variations in the light output of a CsI crystal, the PH depends on the proton hit position. If not compensated for, this effect will contribute with up to half the intrinsic energy resolution in the CsIs. Therefore, a polynomial describing the PH as a function of the vertical hit position is employed instead of a constant value in the PH–energy relation.

The plastic scintillator detectors are calibrated using events where protons hit a narrow, central section of the scintillator, i. e. where the distance is approximately the same to both PM tubes, and where it can be assumed that both of these detect half of the energy deposited. Each PM tube is calibrated separately. The energy represented by the peak channel in a PH spectrum is obtained by calculating the preceding losses, as in the CsI case. A pedestal channel gives a second calibration point for each PM tube, and a linear correspondence is assumed. Finally, the total energy detected by a plastic scintillator is the sum of the energies in the two PM tubes.

The total energy of a particle emitted in the target is obtained by adding the energies from the ΔE and E detectors, as well as the energy loss that the particle undergoes in materials where it is not detected, such as detector wrapping, drift chamber foils and air. The latter contributions are calculated.

5.2.2 Particle identification

A $\Delta E - E$ technique is used to separate protons and deuterons originating in the target. Fig. 6 shows a typical $\Delta E - E$ scatter plot from 96 MeV neutron-induced charged-particle production reactions in carbon and CH_2 in the multitarget box, detected at 7°. Here, ΔE is the sum of the detected energy losses in the two trigger detectors (T1 and T2). The separation between protons and deuterons is good enough to make the assignment of particle ID a straight-forward procedure. Two-dimensional contours can be applied to the scatter plot for both particle types, facilitating the analysis of a specific reaction.

5.2.3 Low-energy neutron rejection

In order to reject low-energy neutrons, the neutron TOF can be constructed. A TDC registers the time difference between the MASTER signal and the cyclotron RF. The measured TOF is thus the sum of the flight times for the neutron and the charged particle. Since the energy of the charged particle is measured, and the particle mass is known by selecting protons or deuterons, its flight time over the known target-to-detector distance can be calculated. Subtraction of the charged-particle flight time from the total, measured TOF then yields the neutron TOF.

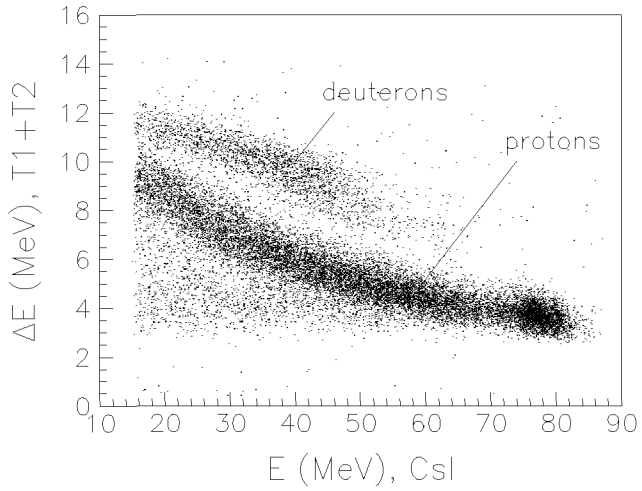

Figure 6: Two-dimensional scatter plot of the sum of the energies detected in the trigger scintillators versus the energy in a CsI detector at 7°. The data are obtained accepting protons from both carbon and CH_2 planes in the multitarget.

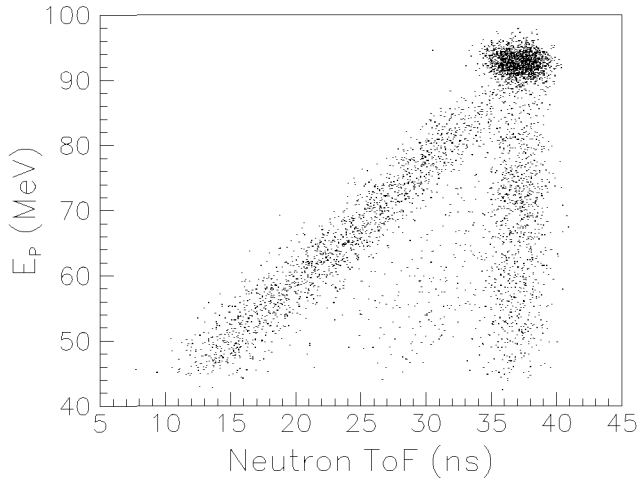

Figure 7: Proton energy versus neutron time-of-flight for (n,p) events, obtained using a CH_2 target. Neutrons corresponding to the full-energy peak appear as a vertical band to the right.

Fig. 7 is a scatter plot of proton energy versus neutron TOF, recorded using a CH_2 target. It illustrates the fact that the full energy neutron peak is accompanied by

a low-energy tail, generating the diagonal band. By making a cut around the full-energy events in the vertical band in the neutron TOF spectrum, the low-energy tail can be reduced. This tail is dominated by protons from H(n,p) reactions, while protons induced by full-energy neutrons, but having energies less than 85 MeV, come from reactions in carbon.

5.2.4 Energy resolution

By normalizing ^{12}C(n,p) spectra with respect to the carbon content in CH_2 and the integrated neutron flux, carbon spectra can be subtracted from those of CH_2, giving pure *np* scattering spectra as illustrated in fig. 8. A TOF rejection of low-energy neutrons has been applied. Furthermore, a gate on proton hit positions on the CsI front area has been employed to ensure that the protons are stopped in the *E* detector, i. e. particles too close to a detector edge are rejected. The hit positions are calculated using drift chamber data.

The resolution of the *np* scattering peak varies due to the differences in intrinsic resolution in the CsI detectors, but an average value of 3.7 MeV (FWHM) has been found. Apart from the CsI detectors, the main contributions to the resolution come from the neutron beam, the plastic scintillators and straggling in non-detector

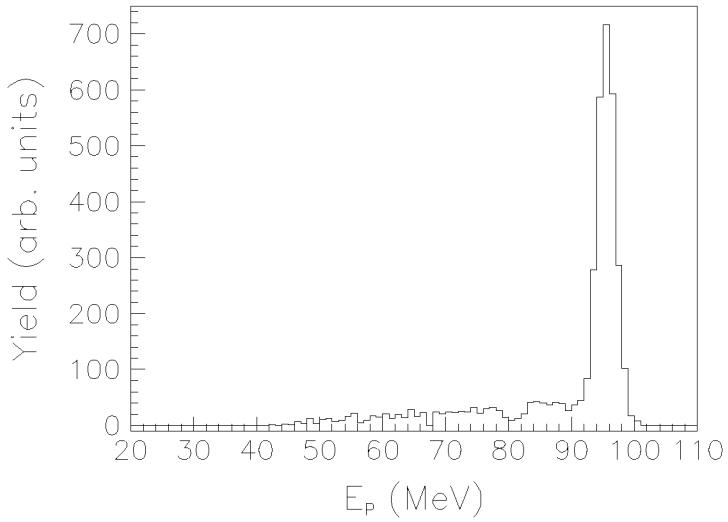

Figure 8: Proton energy spectrum for (n,p) reactions in hydrogen, induced by 96 MeV neutrons, in the angular range 6–7°. The spectrum has been obtained by subtracting a ^{12}C(n,p) spectrum from a proton spectrum coming from CH_2, after normalization.

materials. These are estimated to be 1.2, 1.7 and 0.7 MeV (FWHM), respectively; implying an average intrinsic CsI resolution of 3.0 MeV.

A ^{12}C(n,p) spectrum has been obtained by gating on the carbon planes in the multitarget box. In fig. 9, SCANDAL data are compared with data collected on the same reaction with the LISA spectrometer [31]. For this purpose, LISA data have been folded with a Gaussian representing the resolution in SCANDAL, and data from the SCANDAL measurement have been normalized to the LISA cross section scale. It is obvious that SCANDAL reproduces the data. A low energy cut has been made at 60 MeV, as no low-energy corrections, e. g. for lost particles, are made. The errors are statistical.

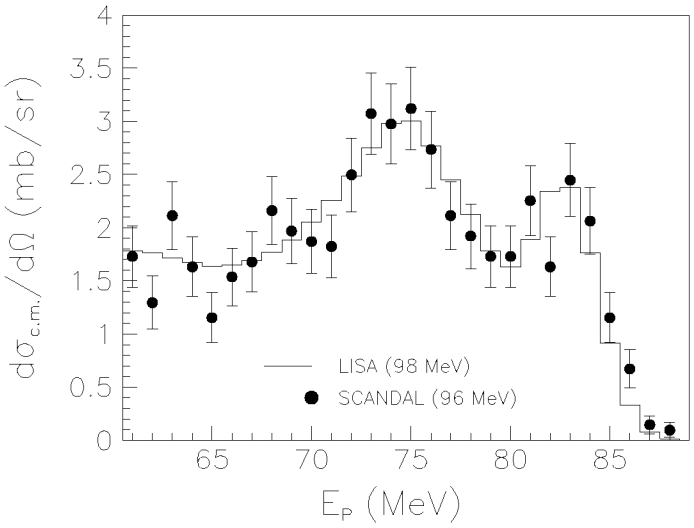

Figure 9: Comparison of SCANDAL and LISA proton energy spectra, from (n,p) reactions in carbon. LISA data have been folded with the SCANDAL resolution, while SCANDAL data have been normalized to the cross section scale of the LISA measurement.

5.3 Neutron mode test experiment

In neutron mode, charged particles contaminating the beam are rejected by the empty multitarget box, while charged particles produced in the scattering target are rejected by the veto detector.

Particle identification is used to separate protons from deuterons, both originating in neutron-induced reactions in the converter. Furthermore, in order to accept protons due to conversion via H(n,p) reactions, and reject those coming from carbon, a maximum opening angle criterion is applied (see section 4).

5.3.1 SCANDAL response function

Fig. 10 shows excitation energy spectra for ^{12}C(n,n) at 96 MeV and 9° scattering angle. A maximum opening angle of 10° has been employed for the (n,p) conversion. The large peak at $E_X = 0$ MeV is due to elastic scattering, and the excited states at 9.6 MeV, and possibly at 4.4 MeV, are small but visible.

A response function for the SCANDAL setup has been constructed. The upper plot of fig. 10 shows different components of this function. A Gaussian has been fitted to the H(n,p) peak in the converter, reflecting elastic scattering from the ground state in ^{12}C. Knowing the relative cross section of ^{12}C(n,p) reactions in the converter with respect to that of (n,p) reactions in hydrogen, a ^{12}C(n,p) spectrum

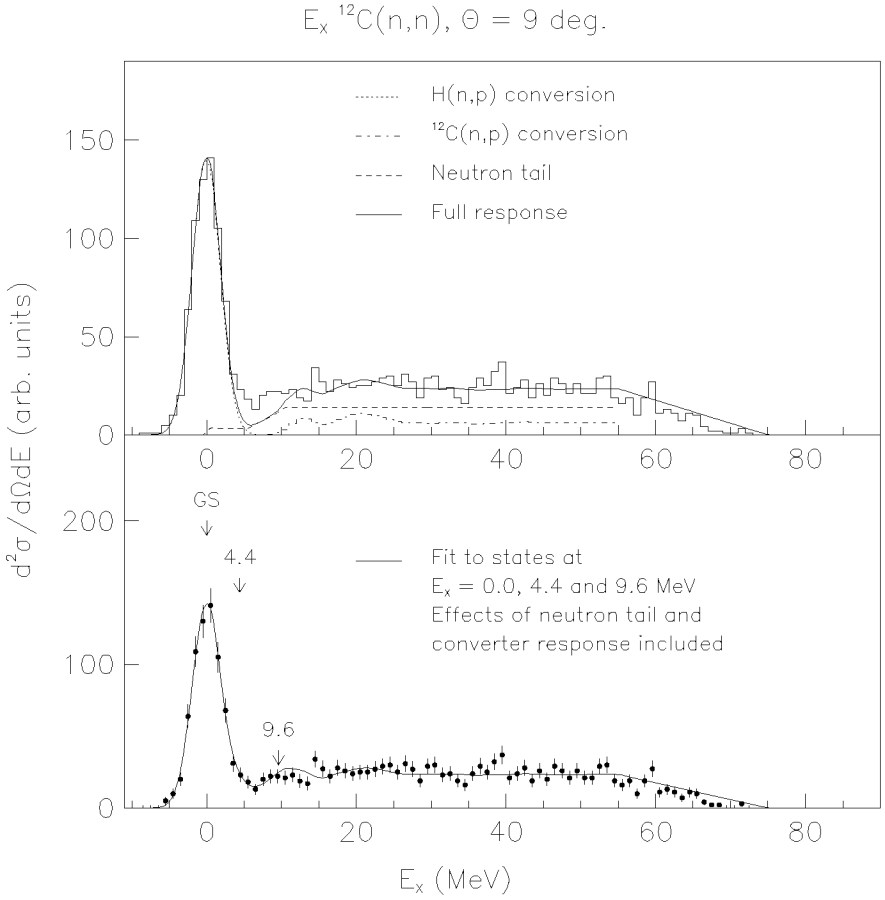

Figure 10: Excitation energy spectra for ^{12}C(n,n) at 9°. See the text for details on the response function and its contributions.

has been added. Also, a low-energy neutron tail has been included by knowing the ^{7}Li(p,n) cross section, again with respect to that of H(n,p) in the converter.

At an excitation energy of 75 MeV, the energy of the scattered neutron is 20 MeV, giving an energy of 0–10 MeV for the protons reaching the CsI detector. Protons with these energies are rejected in the analysis; thus there are no events in the E_X spectrum above 75 MeV. For $E_X = 55$ MeV, the resulting proton energies are high enough for all events to be recorded. Thus, a straight line describing the cut-off at high excitation energies has been employed between $E_X = 55$ and 75 MeV.

Adding the contributions from the hydrogen peak, the ^{12}C(n,p) and the low-energy neutron backgrounds, as well as the cut-off at high E_X, gives the full response function shown in the upper plot.

In the lower plot of fig. 10, Gaussians have been fitted to the excited states at 4.4 and 9.6 MeV, in addition to the ground state fit. Contributions from ^{12}C(n,p) reactions in the converter and from the low-energy neutron tail, relative to these states, have been included in the response function.

It is concluded that the full spectrum can be explained in terms of the effects described here, and that no unexpected contributions are seen.

The energy resolution is 3.7 MeV (FWHM), as shown in section 4.

5.3.2 Detection efficiency

The detection efficiency of the SCANDAL setup consists of the probability for a H(n,p) reaction to take place in the converter, i. e. the conversion efficiency, and the efficiency of detecting the proton.

The probability for a conversion in hydrogen is obtained by integrating the cross section for the H(n,p) reaction over the solid angle given by the maximum opening angle criterion. As was mentioned in section 4, for a converter thickness of 1 cm and a maximum opening angle of 15°, the conversion efficiency is estimated to be $5 \cdot 10^{-4}$.

The detection efficiency has contributions from the efficiencies in each drift chamber plane (four per SCANDAL arm), the efficiency of selecting the correct wire when there are double-hit events in the drift chambers, the CsI response (see below), and reaction losses of neutrons in the target. The contributions are measured or estimated to be 0.75 (from an average of 0.93 per plane, as discussed in section 4), 0.93, 0.92, and 0.93, respectively. This makes a total proton detection efficiency of 0.60.

5.4 CsI response measurement

There is a finite probability that a proton stopping in CsI undergoes a nuclear reaction before coming to rest. Since the light yield is smaller for other ions than protons, this results in loss of light, which manifests itself as a tail in the response function.

This effect has been studied experimentally using H(n,p) data at small angles. By applying gates on energy loss in the trigger scintillators and on incident neutron energy (via time of flight), data sets with a limited range of proton energies incident on the CsI detectors were defined. The response, i. e. the pulse height distribution, for the same data in the CsI crystals display a full-energy peak and a tail.

This behaviour has been modeled by assuming that all nuclear reactions result in total light loss. Thereby, the experimentally well-known total reaction cross section can be used for an estimation of this effect. In general, good agreement between the data and this simple model has been found, as can be seen in fig. 11. Hence, the line in the figure is not a fit to the measured data.

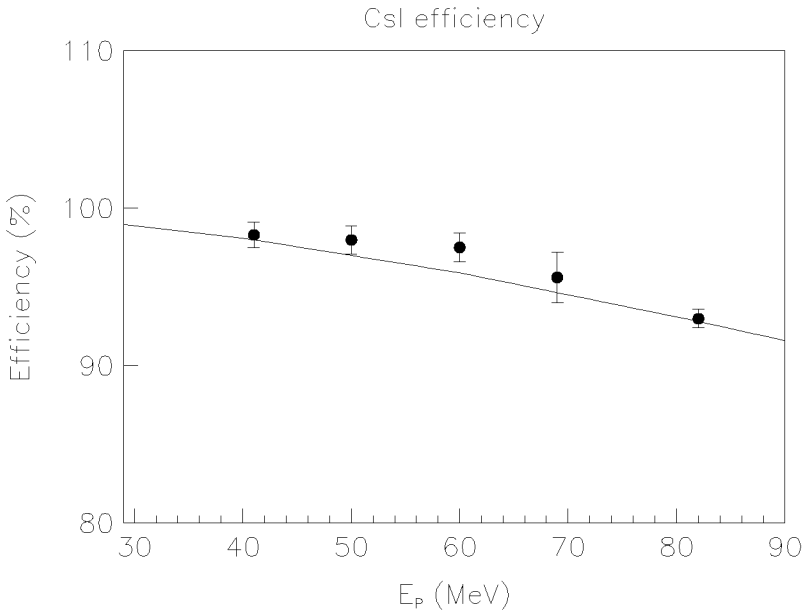

Figure 11: The experimentally determined energy dependence of the CsI full-energy peak efficiency. The line is due to a model based on the reaction cross section. See the text for details.

5.5 Normalization

Normalization of neutron-induced cross sections is a notorious problem because of the difficulties in monitoring the absolute intensity of neutron beams. Precisions better than 10 % have very rarely been achieved. Therefore, most data have been measured relative to another cross section assumed to be known. Most often, the neutron-proton scattering cross section has been used as the primary standard.

Recent experimental investigations [35, 36, 37, 38] have indicated that the *np* scattering cross section above 50 MeV might have larger uncertainties than previously estimated. It seems now that the cross section can be uncertain by as much as 10–15 % in the energy range of 100 MeV and up [45].

A recent high-precision measurement of *np* scattering at 96 MeV in the 74–180 degree range claims an absolute uncertainty of 1.9 % [38], but this is outside our angular range. This is where the planned H(n,n) measurement comes in. By making a relative measurement of the angular distribution of H(n,n) from (close to) zero degrees and out to angles overlapping with the existing data, a normalization to the total cross section can be made with a very small uncertainty (about 1 %) [46].

The reason for this high precision is that the total cross section has been possible to determine with a very high precision (1 %), because knowledge of the absolute beam intensity is not required. Instead, it can be inferred from intensity ratio measurements in attenuation experiments. Furthermore, in the case of hydrogen, integration of the elastic scattering cross section accounts for more than 99 % of the total cross section, with very small corrections for capture and bremsstrahlung processes.

For practical experimental reasons, we plan to measure this in a CH_2-vs-C difference measurement. By this technique, we can normalize the C(n,n) cross section to the H(n,n) cross section. This is very useful, because thereby we can establish the much larger C(n,n) cross section as a secondary standard, allowing all other nuclei to be measured relative to C(n,n).

A second normalization method will be provided by comparisons with the total elastic cross section. This cross section has been derived from the difference of the total cross section and the total inelastic cross section. Both these quantities have been measured in attenuation experiments, and are therefore known to high precision, i. e. 1–2 %. (See for example ref. [47]). By covering 0–70 degrees, far more than 99 % of the contribution to the total elastic cross section will be accounted for, providing a second normalization technique. This method works the best with light nuclei, and is therefore well suited for e. g. C(n,n), but is not as reliable for ^{208}Pb(n,n). Hence, this is another reason to establish C(n,n) as a secondary standard. A detailed account of these issues is underway [48].

6 Experimental programme

Given the time and cost to carry out elastic scattering experiments, the main focus must be on developing theoretical models rather than systematically measuring all nuclei. The obvious nuclei to study are then the magic or semi-magic nuclei, i.e. ^{12}C, ^{16}O, ^{40}Ca, ^{90}Zr and ^{208}Pb. Here it is fortunate that lead and zirconium are also important materials in future transmutation facilities, and carbon, oxygen and calcium are all of direct medical and dosimetric relevance, so the gain is twofold. Besides the elements above, H(n,n) will be studied for normalization purposes. Important materials for transmutation cores, like iron, chromium, bismuth, thorium and uranium might be investigated in a second phase.

Studies of (n,xp) reactions on nuclei of interest for transmutation applications are carried out using SCANDAL in proton mode [49]. Data on ^{208}Pb and ^{56}Fe have been acquired, and experiments on ^{238}U are planned.

A programme to study (n,xn) reactions is underway [50], i.e. neutron emission spectra over a wide secondary energy range. For this project, a new multi-layer converter is being developed, allowing the conversion from ^{12}C(n,p) to be subtracted.

The large solid angle and versatile operation of SCANDAL allows it to be used also for other applications. Recently, parts of SCANDAL were employed as proton detector in a tagged-neutron measurement of the absolute efficiency in the 20–100 MeV range of liquid neutron detectors [51]. This experiment did not only provide an overall efficiency determination, but the spatial efficiency variation could also be mapped, for the first time at these energies.

7 Summary and conclusions

In this paper, we have presented the new SCANDAL facility (SCAttered Nucleon Detection AssembLy), intended for measurements of elastic neutron scattering in the 50–130 MeV range, but also useful for (n,xp) studies in the same energy range. Such data are relevant for applications in transmutation technologies, spallation neutron sources, fast-neutron cancer therapy, dosimetry, neutron-induced electronics failures as well as in basic physics. The neutron production facility is also described in some detail.

The setup consists of two identical detection systems, each having a veto scintillator for fast charged-particle rejection, a plastic scintillator neutron-to-proton converter, two plastic scintillators for triggering and particle identification, two drift chambers for proton tracking, and an array of CsI detectors for energy determination.

The facility subtends a very large solid angle, making experiments with reasonable count rates possible in the first place. It can be used to acquire data with good energy and angular resolutions, very small background, and very good particle

identification. In addition, the timing properties allow suppression of events due to the low-energy neutron tail. When employed for proton detection, simultaneous studies of up to seven targets can be accomplished by means of a segmented target device.

The performance of the facility is illustrated with data from experiments on neutron and proton emission from carbon and CH_2 targets at 96 MeV incident neutron energy.

Acknowledgements

We wish to thank the technical staff of the The Svedberg Laboratory for enthusiastic and skillful assistance, especially Olle Byström, Sture Hultqvist, Johan Nyberg and Tore Sundqvist. Thanks are also due to the CELSIUS/WASA collaboration for co-operation on the CsI detectors. The special practical support of Frida Boserius, Sara Svedbro, Jan Johansson, Nils Gollub and Matthias Holz is gratefully acknowledged.

This work was financially supported by Vattenfall AB, Swedish Nuclear Fuel and Waste Management Company, Swedish Nuclear Power Inspectorate, Barsebäck Power AB, Swedish Defence Research Establishment, Swedish Natural Science Research Council, and the European Commission.

References

[1] Proceedings of the 3rd International Conference on Accelerator Driven Transmutation Technologies (ADTTA99), Prague, Czech Republic, June 7-11, 1999. www.fjfi.cvut.cz/con_adtt99/.

[2] A. Wambersie, P. Pihet, H.G. Menzel, Radiat. Prot. Dosim. **31** (1990) 421.

[3] M. Tubiana, J. Dutreix, A. Wambersie, Introduction to Radiobiology (Taylor & Francis, 1990).

[4] J.F. Ziegler, IBM J. Res. Develop. **40** (1996) 19.

[5] H.H.K. Tang, IBM J. Res. Develop. **40** (1996) 91.

[6] D. O'Sullivan, private communication. EU Cosmic Radiation and Dosimetry Group.

[7] Proceedings of Workshop on Critical Issues in the Determination of the Pion-Nucleon Coupling Constant, ed. J. Blomgren, Physica Scripta T87 (2000).

[8] R.W. Finlay, W.P. Abfalterer, G. Fink, E. Montei, T. Adami, P.W. Lisowski, G.L. Morgan, R.C. Haight, Phys. Rev. C **47** (1993) 237.

[9] J. Rapaport and E. Sugarbaker, Annu. Rev. Nucl. Part. Sci. **44** (1994) 109.

[10] W.P. Alford and B.M. Spicer, Advances in Nuclear Physics **24** (1998) 1.

[11] E.L. Hjort, F.P. Brady, J.L. Romero, J.R. Drummond, D.S. Sorenson, J.H. Osborne, B. McEachern, L.F. Hansen, Phys. Rev. C **50** (1994) 275.

[12] J. Rapaport, private communication. J. Osborne, thesis, unpublished.

[13] R.W. Finlay, private communication. *Proposal to the NSF for the support of CHICANE/SPECTROMETER SYSTEM FOR THE IUCF COOLER RING*, (1992).

[14] H. Condé, S. Hultqvist, N. Olsson, T. Rönnqvist, R. Zorro, J. Blomgren, G. Tibell, A. Håkansson, O. Jonsson, A. Lindholm, L. Nilsson, P.-U. Renberg, A. Brockstedt, P. Ekström, M. Österlund, F.P. Brady, Z. Szeflinski, Nucl. Instr. Meth. **A292** (1990) 121.

[15] P.W. Lisowski, C.D. Bowman, G.J. Russell, S.A. Wender, Nucl. Sci. Eng. **106** (1990) 208.

[16] W. Hürster, Th. Fischer, G. Hammel, K. Kern, M. Kleinschmidt, L. Lehmann, H. Schmitt, L. Schmitt, D.M. Sheppard, Phys. Lett. **B90** (1980) 367.

[17] E. Radermacher, private communication. C. Rubbia, S. Andriamonje, D. Bouvet-Bensimon, S. Buono, R. Cappi, P. Cennini, C. Gelès, I. Goulas, Y. Kadi, P. Pavlopoulos, J.P. Revol, A. Tzima, V. Vlachoudis, CERN internal report CERN/LHC/98-02.

[18] J.A. Jungerman and F.P. Brady, Nucl. Instr. Meth. **89** (1970) 167.

[19] S.S. Hanna, C.J. Martoff, D. Pocanić, K. Wang, R.C. Byrd, C.C. Foster, I.J. van Heerden, Nucl. Instr. Meth. **A401** (1997) 345.

[20] R. Helmer, Can. J. Phys. **65** (1987) 588.

[21] W.R. McMurray, D.G. Aschman, K. Bharuth-Ram, R.W. Fearick, Nucl. Instr. Meth. **A329** (1993) 217.

[22] M. Baba, Y. Nauchi, T. Iwasaki, T. Kiyosumi, M. Yoshioka, S. Matsuyama, N. Hirakawa, T. Nakamura, Su. Tanaka, S. Meigo, H. Nakashima, Sh. Tanaka, N. Nakao, Nucl. Instr. Meth. **A428** (1999) 454.

[23] H. Schuhmacher, H.J. Brede, V. Dangendorf, M. Kuhfuss, J.P. Meulders, W.D. Newhauser, R. Nolte, Nucl. Instr. Meth. **A421** (1999) 284.

[24] N. Nakao, Y. Uwamino, T. Nakamura, T. Shibata, N. Nakanishi, M. Takada, E. Kim, T. Kurosawa, Nucl. Instr. Meth. **A420** (1999) 218.

[25] T. Peterson, Impact on the πNN Coupling Constant of the IUCF Measurement with a Tagged Neutron Beam, in Proceedings of Workshop on Critical Issues in the Determination of the Pion-Nucleon Coupling Constant, Physica Scripta T87 (2000) 22 [7].

[26] A.N. Smirnov, V.P. Eismont, A.V. Prokofiev, Rad. Meas. **25** (1995) 151.

[27] L. Tommasino, N. Klein, P. Solomon, J. Appl. Phys. **46**, No. 4 (1975) 1484.

[28] R.C. Byrd and W.C. Sailor, Nucl. Instr. Meth. **A264** (1989) 494.

[29] S. Dangtip, J. Blomgren, N. Olsson, H. Condé, K. Elmgren, J. Rahm, A. Ringbom, G. Tibell, O. Jonsson, L. Nilsson, P.-U. Renberg, S.Y. van der Werf, Nucl. Phys. **A677** (2000) 3.

[30] A. Ringbom, G. Tibell, J. Blomgren, H. Condé, K. Elmgren, N. Olsson, J. Rahm, T. Rönnqvist, O. Jonsson, L. Nilsson, P.-U. Renberg, Chr. Bargholtz, K. Fransson, K. Lindh, P.-E. Tegnér, P. Thörngren-Engblom, S.Y. van der Werf, Nucl. Phys. **A679** (2000) 231.

[31] N. Olsson, H. Condé, E. Ramström, T. Rönnqvist, R. Zorro, J. Blomgren, A. Håkansson, G. Tibell, O. Jonsson, L. Nilsson, P.-U. Renberg, A. Brockstedt, P. Ekström, M. Österlund, S.Y. van der Werf, D.J. Millener, G. Szeflinska, Z. Szeflinski, Nucl. Phys. **A559** (1993) 368.

[32] T. Rönnqvist, H. Condé, N. Olsson, E. Ramström, R. Zorro, J. Blomgren, A. Håkansson, A. Ringbom, G. Tibell, O. Jonsson, L. Nilsson, P.-U. Renberg, S.Y. van der Werf, W. Unkelbach, F.P. Brady, Nucl. Phys. **A563** (1993) 225.

[33] H. Condé, N. Olsson, E. Ramström, T. Rönnqvist, R. Zorro, J. Blomgren, A. Håkansson, G. Tibell, O. Jonsson, L. Nilsson, P.-U. Renberg, M. Österlund, W. Unkelbach, J. Wambach, S.Y. van der Werf, J. Ullmann, S.A. Wender, Nucl. Phys. **A545** (1992) 785.

[34] A. Ringbom, A. Håkansson, G. Tibell, R. Zorro, J. Blomgren, H. Condé, N. Olsson, J. Rahm, E. Ramström, T. Rönnqvist, O. Jonsson, L. Nilsson, P.-U. Renberg, S.Y. van der Werf, H. Lenske, Nucl. Phys. **A617** (1997) 316.

[35] T. Rönnqvist, H. Condé, N. Olsson, R. Zorro, J. Blomgren, G. Tibell, O. Jonsson, L. Nilsson, P.-U. Renberg, S.Y. van der Werf, Phys. Rev. **C45** (1992) R496.

[36] T.E.O. Ericson, B. Loiseau, J. Nilsson, N. Olsson, J. Blomgren, H. Condé, K. Elmgren, O. Jonsson, L. Nilsson, P.-U. Renberg, A. Ringbom, T. Rönnqvist, G. Tibell, R. Zorro, Phys. Rev. Lett. **75** (1995) 1046.

[37] J. Rahm, J. Blomgren, H. Condé, S. Dangtip, K. Elmgren, N. Olsson, T. Rönnqvist, R. Zorro, A. Ringbom, G. Tibell, O. Jonsson, L. Nilsson, P.-U. Renberg, T.E.O. Ericson, B. Loiseau, Phys. Rev. **C57** (1998) 1077.

[38] J. Rahm, J. Blomgren, H. Condé, K. Elmgren, N. Olsson, T. Rönnqvist, R. Zorro, A. Ringbom, G. Tibell, O. Jonsson, L. Nilsson, P.-U. Renberg, T.E.O. Ericson, B. Loiseau, *np* scattering measurements at 96 MeV, (in manuscript).

[39] S. Dangtip, A. Ataç, B. Bergenwall, J. Blomgren, K. Elmgren, C. Johansson, J. Klug, N. Olsson, G. Alm Carlsson, J. Söderberg, O. Jonsson, L. Nilsson, P.-U. Renberg, P. Nadel-Turonski, C. Le Brun, F.R. Lecolley, J.F. Lecolley, C. Varignon, Ph. Eudes, F. Haddad, M. Kerveno, T. Kirchner, C. Lebrun, Nucl. Instr. Meth. **A452** (2000) 484.

[40] V.P. Eismont, A.V. Prokofiev, A.N. Smirnov, K. Elmgren, J. Blomgren, H. Condé, J. Nilsson, N. Olsson, T. Rönnqvist, E. Tranéus, Phys. Rev. **C53** (1996) 2911.

[41] K. Johansson, P. Dyreklev, B. Granbom, N. Olsson, J. Blomgren, P.-U. Renberg, IEEE transactions on Nuclear Science I **45** (1998) 2519.

[42] K. Johansson, M. Ohlsson, N. Olsson, J. Blomgren, P.-U. Renberg, IEEE transactions on Nuclear Science I **46** (1999) 1427.

[43] B. Höistad, E. Nilsson, J. Thun, S. Dahlgren, S. Isaksson, G.S. Adams, H. Ikegami, Nucl. Instr. Meth. **A295** (1990) 172.

[44] T. Sundqvist and J. Nyberg, TSL Progress Report 1996-1997, p. 21.

[45] J. Blomgren, N. Olsson, J. Rahm, How Strong is the Strong Interaction? – The πNN Coupling Constant and the Shape and Normalization of np Scattering Cross Sections, in Proceedings of Workshop on Critical Issues in the Determination of the Pion-Nucleon Coupling Constant, Physica Scripta T87 (2000) 33.

[46] C. Johansson, *et al.*, to be published.

[47] J. DeJuren and N. Knable, Phys. Rev. **77** (1950) 606.

[48] J. Klug, *et al.*, to be published.

[49] J.F. Lecolley, *et al.*, TSL experiment FA118.

[50] J.F. Lecolley, *et al.*, TSL experiment FA131.

[51] J. Thun, J. Källne, C. Varignon, J. Blomgren, F. Borne, K. Elmgren, O. Jonsson, J.F. Lecolley, X. Ledoux, F. Lefebvres, N. Olsson, Y. Patin, P.-U. Renberg, The response of a liquid scintillator detector to neutrons of energies between 21 and 100 MeV, to be published.